New Phytologist

Methods

Sapflow+: a four-needle heat-pulse sap flow sensor enabling nonempirical sap flux density and water content measurements

Maurits W. Vandegehuchte and Kathy Steppe

Laboratory of Plant Ecology, Faculty of Bioscience Engineering, Ghent University, Coupure links 653, 9000 Gent, Belgium

Author for correspondence:
Maurits W. Vandegehuchte
Tel: +32 9 264 61 26
Email: maurits.vandegehuchte@ugent.be

Received: *6 April 2012*
Accepted: *11 June 2012*

New Phytologist (2012) **196**: 306–317
doi: 10.1111/j.1469-8137.2012.04237.x

Key words: heat capacity, heat pulse, moisture content, sap flow, sap flux density, sensor, thermal conductivity, thermal diffusivity.

Summary

- To our knowledge, to date, no nonempirical method exists to measure reverse, low or high sap flux density. Moreover, existing sap flow methods require destructive wood core measurements to determine sapwood water content, necessary to convert heat velocity to sap flux density, not only damaging the tree, but also neglecting seasonal variability in sapwood water content.
- Here, we present a nonempirical heat-pulse-based method and coupled sensor which measure temperature changes around a linear heater in both axial and tangential directions after application of a heat pulse. By fitting the correct heat conduction–convection equation to the measured temperature profiles, the heat velocity and water content of the sapwood can be determined.
- An identifiability analysis and validation tests on artificial and real stem segments of European beech (*Fagus sylvatica* L.) confirm the applicability of the method, leading to accurate determinations of heat velocity, water content and hence sap flux density.
- The proposed method enables sap flux density measurements to be made across the entire natural occurring sap flux density range of woody plants. Moreover, the water content during low flows can be determined accurately, enabling a correct conversion from heat velocity to sap flux density without destructive core measurements.

Introduction

Accurate measurements of sap flux density and stem water content are of major importance in understanding and quantifying plant–water relations, and hence in hydrological and climatological studies, ecosystem research, irrigation practices, colonization by fungi and insects, plant growth, fertilization, stress monitoring and forestry. At present, the sap flux density and stem water content can be measured simultaneously by magnetic resonance imaging (Van As *et al.*, 2009), but this laboratory technique is expensive, necessitates specific tuning for different flow ranges and remains difficult to apply in the field despite recent progress (Jones *et al.*, 2012). Although many methods have been developed to determine the sap flux density or stem water content separately, to our knowledge, no practically applicable method exists which combines both.

From thermodynamics, it is known that heat dispersion in sapwood is dependent on the specific heat capacity and thermal conductivity of the sapwood, which are both influenced by the stem water content and sap flux density. Therefore, since the first application of heat as a tracer in sapwood (Huber, 1932), many methods based on thermodynamic principles have been developed to determine the sap flux density (Marshall, 1958; Cohen *et al.*, 1981; Swanson & Whitfield, 1981; Swanson, 1983; Granier, 1985; Nadezhdina *et al.*, 1998; Burgess *et al.*, 2001; Green *et al.*, 2003; Clearwater *et al.*, 2009; Testi & Villalobos, 2009). For these methods, a distinction can be made between those which continuously heat the sapwood and empirically link a measured temperature ratio to the sap flux density, and those which apply heat pulses to determine the heat velocity, based on the isotropic heat conduction–convection equation as mentioned in Marshall (1958), and necessitate a measurement of the water content to convert the heat velocity to the sap flux density.

Although each of these methods has its merits in sap flow research, they all have their specific limitations. For those applying heat continuously, the heat field deformation (HFD) method (Nadezhdina *et al.*, 1998, 2012) and thermal dissipation probe (TDP) (Granier, 1985) are most often employed. Although the HFD method enables sap flux density measurements to be made

at different depths in the sapwood and is capable of distinguishing high, low and reverse flows, it remains empirical and can lead to over- or underestimations depending on the sap flux density, water content and thermal characteristics of the wood (Vandegehuchte & Steppe, 2012b). The TDP method suffers from these same limitations and is known to largely underestimate the sap flux density (Steppe *et al.*, 2010).

For the heat-pulse methods, the compensation heat-pulse method (CHPM) has the advantage that the thermal diffusivity does not need to be determined. However, it is incapable of determining low and reverse flows (Becker, 1998; Green *et al.*, 2009; Steppe *et al.*, 2010). This was partly resolved by Testi & Villalobos (2009), who used the average temperature gradient (calibrated average gradient method), extending measurement possibilities towards the lower sap flow range. This method, however, necessitates an empirical calibration which is dependent on the thermal characteristics of the sapwood. The heat ratio method (HRM) (Burgess *et al.*, 2001) can measure both low and reverse flows, but performs poorly at high flow rates (Burgess & Dawson, 2008), and applies an inaccurate protocol to determine the thermal diffusivity, necessary as an input parameter for sap flux density calculations (Vandegehuchte & Steppe, 2012a). The Tmax method (Cohen *et al.*, 1981) determines the thermal diffusivity correctly, but is based on a single point analysis and is hence susceptible to scatter. Moreover, like CHPM, it is unable to correctly estimate low and reverse flows (Green *et al.*, 2009). For all these heat-pulse methods, the measurement and heater needles are inserted in the sapwood. This invasive character of the sensors creates a sapwood zone in which flow is interrupted, the so-called 'wound effect'. This effect leads to an underestimation of the calculated heat velocity which can be corrected for by determining a wound correction equation based on thermodynamic modelling of the heat transport in the sapwood (Swanson & Whitfield, 1981).

As heat-pulse methods determine the heat velocity, a knowledge of the water content and dry wood density is necessary to obtain the sap flux density:

$$q_s = \frac{\rho_d}{\rho_s}\left(MC + \frac{c_{dw}}{c_s}\right) V_h \qquad \text{Eqn 1}$$

(q_s, sap flux density ($m^3\ m^{-2}\ s^{-1}$); V_h, heat velocity ($m\ s^{-1}$); MC, sapwood water content (kg water (kg dry weight)$^{-1}$); c_{dw}, specific heat capacity of dry wood (1200 J $kg^{-1}\ K^{-1}$; Edwards & Warwick, 1984); ρ_d, dry density of sapwood ($kg\ m^{-3}$); ρ_s, density of the sap (assumed to be the density of water, 1000 kg m^{-3}); c_s, specific heat capacity of the sap (assumed to be that of water, 4186 J $kg^{-1}\ K^{-1}$; Edwards & Warwick, 1984)). A full list of symbols used in the article can be found in Table 1. MC and ρ_d can be determined by taking a wood core. Although ρ_d will remain approximately equal for a specific tree, MC is known to vary both seasonally and daily, with annual changes of up to 70% and more depending on species and environment (Skaar, 1988; Wullschleger *et al.*, 1996; Nadler *et al.*, 2008). Hence, if MC is only determined once, this might induce large errors in the sap flux density obtained. Although relative changes in stem water content can be estimated by applications of methods, such as time domain reflectometry, resistivity tomography, γ-ray attenuation and electrical resistance, these methods require additional equipment, are difficult to interpret and struggle to take into account the spatial variability of the sapwood (Wullschleger *et al.*, 1996; Nadler & Tyree, 2008; Bieker & Rust, 2012).

Our study describes a new type of method and coupled sensor, referred to as Sapflow+, capable of the nondestructive measurement of high, low and reverse sap flows, thermal wood properties and water content of the sapwood based on thermodynamics. A theory is presented to determine these parameters based on the conduction and convection of a short-duration heat pulse away from an infinite line source in the sapwood. It is shown that, by using this theory, sap flow, thermal wood properties and water content can be determined by a four-needle probe. Results of both finite element modelling and laboratory experiments are presented which demonstrate the applicability of the theory for the measurement of the sap flux density and water content of fresh sapwood.

Table 1 List of symbols

Symbol	Unit	Explanation
V_h	$m\ s^{-1}$	Heat velocity
q_s	$m^3\ m^{-2}\ s^{-1}$	Sap flux density
K	$W\ m^{-1}\ K^{-1}$	Thermal conductivity
c	$J\ kg\ K^{-1}$	Heat capacity
ρ	$kg\ m^{-3}$	Density
ρc	$J\ m^{-3}\ K^{-1}$	Volumetric heat capacity
D_{ax}	$m^2\ s^{-1}$	Axial thermal diffusivity
D_{tg}	$m^2\ s^{-1}$	Tangential thermal diffusivity
K_{ax}	$W\ m^{-1}\ K^{-1}$	Axial thermal conductivity
K_{tg}	$W\ m^{-1}\ K^{-1}$	Tangential thermal conductivity
q	$W\ m^{-1}$	Heat given off per unit length of the heat source
x	m	Distance between the heater needle and the axial needle
y	m	Distance between the heater needle and the tangential needle
ΔT	K	Temperature difference between the temperature during or after application of the heat pulse at a time t and the temperature before application of the heat pulse at a certain position (x,y) from the heater
T	K	Temperature at a certain position (x,y) from the heater
w_d	kg	Oven dry weight
w_f	kg	Fresh weight
c_w	$J\ kg^{-1}\ K^{-1}$	Specific heat capacity of water
c_d	$J\ kg^{-1}\ K^{-1}$	Specific heat capacity of dry wood
K_w	$W\ m^{-1}\ K^{-1}$	Thermal conductivity of water
K_d	$W\ m^{-1}\ K^{-1}$	Thermal conductivity of dry wood
MC		Water content (moisture to dry weight)
ρ_w	$kg\ m^{-3}$	Density of water
ρ_d	$kg\ m^{-3}$	Density of dry wood (sapwood after drying)
K_d	$W\ m^{-1}\ K^{-1}$	Thermal conductivity of dry wood
F_v		Void fraction of the wood
t_m	s	Time from the start of the heat pulse until the maximal temperature rise
t_0	s	Duration of the heat pulse

Materials and Methods

Theory

The theory applied is developed for an infinitely long linear heater of zero radius in an infinitely large medium. Based on the work of Kluitenberg & Ham (2004) and Vandegehuchte & Steppe (2012c), the temperature distribution in an anisotropic medium is expressed as:

$$\Delta T = \frac{q}{4\pi\sqrt{K_{ax}K_{tg}}}\int_0^t \frac{1}{t}\exp\left(\frac{\rho c}{4t}\left(\frac{(x-V_h^t)^2}{K_{ax}}+\frac{y^2}{K_{tg}}\right)\right)dt \quad \text{for } 0<t<t_0 \qquad \text{Eqn 2}$$

$$\Delta T = \frac{q}{4\pi\sqrt{K_{ax}K_{tg}}}\int_{t-t_0}^t \frac{1}{t}\exp\left(\frac{\rho c}{4t}\left(\frac{(x-V_h^t)^2}{K_{ax}}+\frac{y^2}{K_{tg}}\right)\right)dt \quad \text{for } t_0<t \qquad \text{Eqn 3}$$

(ΔT, temperature difference (K) between the measured temperature at time t (s) after application of the pulse and the measured temperature before the heat pulse, measured at a distance x (m) axial and y (m) tangential from the heater, respectively; K_{ax}, axial thermal conductivity (W m^{-1} K^{-1}); K_{tg}, tangential thermal conductivity (W m^{-1} K^{-1}); ρ, density (kg m^{-3}) of the sapwood; c, specific heat capacity of the sapwood (J kg^{-1} K^{-1}); q, energy input per unit length of the heater per unit time (W m^{-1})). By measuring the temperature change ΔT at three different positions around the heater needle, a multiparameter model which solves Eqns 2 and 3 for each position can be fitted to retrieve the parameters of interest, namely K_{ax}, K_{tg}, ρc (the volumetric heat capacity, J m^{-3} K^{-1}) and V_h. In this model, a temperature correction for changing sapwood temperatures independent of the heat pulses is applied. By determining the temperatures before and after the heat pulse, the slope of temperature change is calculated, which is then subtracted from the modelled temperature changes.

This multiparameter model was implemented, simulated and calibrated using the plant modelling software PhytoSim (Phyto-IT BVBA, Mariakerke, Belgium). For model calibration, the simplex method, originally developed by Nelder & Mead (1965), was used to minimize the weighted sum of squared errors between the measured and simulated values of the temperatures. The weighted sum of squared errors objective value for each fit to the axial and tangential temperature data indicates the goodness of fit:

$$\text{WSSE} = \frac{1}{n}\sum_{i=1}^{k}\frac{1}{\sigma^2}\sum_{j=1}^{n}(m_{ij}-y_{ij})^2 \qquad \text{Eqn 4}$$

(WSSE, weighted sum of squared errors objective; k, number of objective variables (three, for each position at which the temperature is measured); σ^2, measurement error variance for objective variable i (for the three temperature measurements, a value of 0.02 for σ was applied, based on the calibration of the thermocouples in a warm water bath); n, number of measurement points for objective variable I; m_{ij}, jth measurement value of objective variable i; y_{ij}, corresponding simulation value).

Water content

If the volumetric heat capacity (ρc, J m^{-3} K^{-1}) of the sapwood is known, its water content (MC, kg water (kg dry weight)$^{-1}$) can be determined directly (Swanson, 1983):

$$\text{MC} = \frac{1}{c_w}\left(\frac{\rho c}{\rho_d} - c_{dw}\right) \qquad \text{Eqn 5}$$

(c_w and c_{dw}, heat capacities of water (4186 J kg^{-1} K^{-1}; Martin & Lang, 1933) and dry wood (1200 J kg^{-1} K^{-1}; Edwards & Warwick, 1984), respectively; ρ_d, dry wood density (kg m^{-3}), which can be measured once by sampling a wood core).

Sensor design

To apply the theory, a needle probe was designed consisting of a linear heater and three measurement needles located at specific distances axially upstream, downstream and tangentially from the heater (Fig. 1). The three stainless steel measurement needles have a length of 35 mm and a diameter of 1.1 mm. In each measurement needle, a copper-constantan thermocouple is located at 20 mm from the needle base. It should be noted that, similar to HRM, thermocouples could be installed at different depths to assess radial differences in the sap flux density. This, however, requires additional logging capacity. As a result of practical

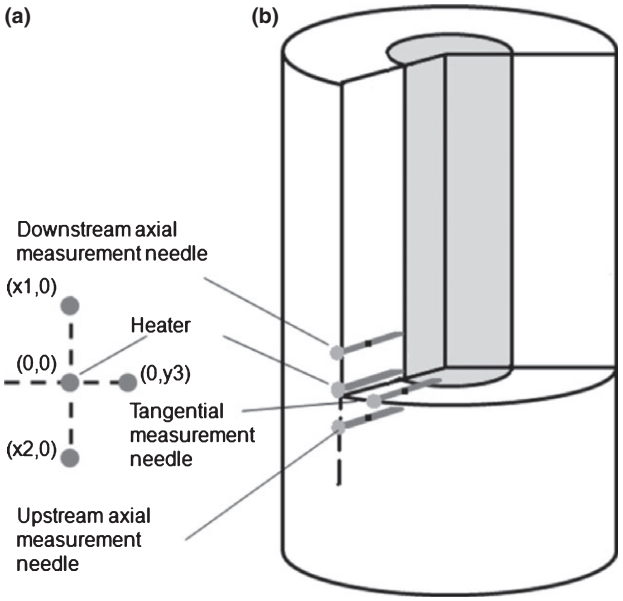

Fig. 1 (a) Schematic diagram of a tangential section of the stem xylem with arrangements of the thermocouples around the heater of the Sapflow+ sensor. (b) Schematic diagram of the Sapflow sensor installed in the sapwood (SW) of a stem.

limitations, in this set-up, it was not possible to install more than one thermocouple in each measurement needle.

The heater needle has a length of 38 mm and a diameter of 1.1 mm. The heater needle is slightly longer than the measurement needles to avoid side effects at the end of the sensor. An enamelled resistance wire with a known resistance (0.02341 Ω mm^{-1}) is coiled around this heater. Heat pulses of 6 s were generated by applying 5 V to the heater. The exact amount of heat released by this heater, q (W m^{-1}), was calculated as described by Campbell *et al.* (1991):

$$q = \left(\frac{U}{R}\right)^2 R' \qquad \text{Eqn 6}$$

(U (V), applied voltage; R (Ω), resistance of the heater; R' (Ω m^{-1}), resistance of the heater per unit length).

A CR1000 datalogger (Campbell Scientific, Loughborough, UK) was used to control the heat pulse, monitor the applied voltage and measure the temperatures as a function of time.

Identifiability analysis

Application of the Sapflow+ model will only be successful when the parameters on which the model is calibrated are identifiable. Therefore, an identifiability analysis, consisting of a sensitivity and a correlation analysis, was conducted for the model parameters ρc, K_{ax}, K_{tg} and V_h. Indeed, a model parameter is said to be identifiable if it has sufficient influence on the model outputs, in this case, the changes in temperature before and after the pulse at three positions around the heater, ΔT_1, ΔT_2 and ΔT_3 (high sensitivity), and, at the same time, is not correlated with other model parameters (no linear dependence on other model parameters) (De Pauw *et al.*, 2008). The equations used for the identifiability analysis can be found in Supporting Information Notes S1.

Sensor verification

A three-dimensional finite element model (FEM) was implemented to compare the theoretical Eqns 2 and 3, developed for a perfect heater (infinite length and zero radius) in an infinitely large environment, with a more realistic situation. To this end, a cube of immobilized water with a length of 10 cm was modelled. In this cube, the three sensor needles and heater were located with their respective dimensions (Fig. S1).

This FEM solves the partial differential equation governing heat transport in each defined node of the three-dimensional structure:

$$\rho c \frac{\partial T}{\partial t} = \vec{K}\left(\frac{\partial^2 T}{\partial x^2} + \frac{\partial^2 T}{\partial y^2} + \frac{\partial^2 T}{\partial z^2}\right) + P \qquad \text{Eqn 7}$$

(T, temperature (K); t, time (s); P, power input (W m^{-3}); ρ, density; c, specific heat capacity; $\vec{K}$, thermal conductivity vector, consisting of radial (K_{rad}), axial (K_{ax}) and tangential (K_{tg}) conductivity, of the medium in which the measurements are conducted). For the immobilized water, values of 1000 kg m^{-3} and 4186 J kg^{-1} K^{-1} were taken for ρ and c, and, for K_{ax}, K_{tg} and K_{rad}, a value of 0.61 W m^{-1} K^{-1} was applied (Martin & Lang, 1933). For the measurement and heater needles, the properties of steel were chosen for implementation in the model (ρ = 7850 kg m^{-3}, c = 475 J kg^{-1} K^{-1}, K = 44.5 W m^{-1} K^{-1}). The outer boundaries of the system were taken at a constant temperature of 20°C. For the inner boundaries of the measurement needles, a continuous heat transfer was considered and, for the heater, a heat source of 160 W m^{-1} was implemented.

These modelling results were then compared with actual measurements in water immobilized with 2 g agar l^{-1} (Campbell *et al.*, 1991; Ren *et al.*, 2003). The small amount of agar was added to prevent natural convection in the water and is assumed to have a negligible effect on the thermal characteristics. This immobilized water has the advantage that it is in direct contact with the heater and needles. From the known thermal properties of this medium, the heat input q, calculated according to Campbell *et al.* (1991), can then be checked for each sensor and a correction factor calculated if necessary.

Comparison of heat pulse methods

In addition to immobilized water, moist wood was modelled according to the same principles and with the same dimensions. The wood was considered to be an anisotropic medium in which unidirectional convection occurred. For this wood, a dry wood density of 550 kg m^{-3} was applied, with varying water content and, accordingly, varying specific heat capacity and thermal conductivity (Vandegehuchte & Steppe, 2012a). In this wood, sap flux densities ranging from − 15 (reverse flow) to 100 cm^3 cm^{-2} h^{-1} (high flow) were modelled. For this model, CHPM, HRM, Tmax and Sapflow+ methods were compared for 6-s heat pulses of 160 W m^{-1}. For the Tmax method, formulae for a nonideal heat pulse, as mentioned in Kluitenberg & Ham (2004), adapted for anisotropic wood, were applied (Eqns 8, 9) (Vandegehuchte & Steppe, 2012c), whereas, for CHPM (Eqn 10) and HRM (Eqn 11), the original equations valid for an ideal heat pulse were applied (Swanson & Whitfield, 1981; Burgess *et al.*, 2001):

$$D_{ax} = \frac{x_1^2}{4t_{m0}} \frac{t_0}{t_{m0} - t_0} \left[\ln\left(\frac{t_{m0}}{t_{m0} - t_0}\right)\right]^{-1} \qquad \text{Eqn 8}$$

$$V_h = \sqrt{\frac{4D_{ax}}{t_0}\ln\left(1 - \frac{t_0}{t_m}\right) + \frac{x_1^2}{t_m(t_m - t_0)}} \qquad \text{Eqn 9}$$

$$V_h = (x_1 + x_2)/(2t_c) \qquad \text{Eqn 10}$$

$$V_h = (D_{ax}/x)\ln(\Delta T_{down}/\Delta T_{up}) \qquad \text{Eqn 11}$$

(x_1 and x_2 taken at 10 mm downstream and 5 mm upstream of the heater, respectively; t_c, time at which ΔT at x_1 and x_2 is equal; t_m, time at which ΔT at x_1 is maximal (with t_{m0} at zero flow); D_{ax}, axial thermal diffusivity ($m^2\ s^{-1}$); ΔT_{down} and ΔT_{up}, temperature differences measured at x mm downstream and upstream, respectively, with x taken at 5 mm).

For both HRM and CHPM, the original equations are theoretically not applicable for nonideal pulses. For HRM, however, it was mentioned in Burgess *et al.* (2001) that there is no significant difference when applying heat pulses of 6 s relative to shorter pulses. This was also confirmed by comparing the theoretical results when applying the original HRM equation to the temperatures modelled by Eqns 2 and 3 for heat pulses ranging between 1 and 10 s. As no significant difference between these results was obtained, the original HRM equation was deemed valid for pulses of 6 s. For CHPM, however, an underestimation of 15% was noted when theoretically applying the ideal heat pulse equation for nonideal heat pulses of 6 s. This underestimation needs to be taken into account when interpreting the results.

As all methods are based on the insertion of needles in the wood, distinction was made between wood without and with wound effects, the latter modelled as regions surrounding the sensor needles in which zero flow occurs with a width of 1.5 mm. This wound effect simulates the interruption of flow caused by the invasiveness of the needles and will lead to a diversion from the ideal condition on which all mentioned methods are based, namely a uniform flow distribution in the wood. This leads to underestimations in the calculated heat velocities. Based on the modelling results, however, a correction can be developed to take into account these wound effects (Swanson & Whitfield, 1981).

Measurements of the sap flux density in artificial sapwood

The Sapflow+ method was tested on an artificial stem segment, consisting of a plastic cylinder filled with fine sawdust of European beech (*Fagus sylvatica* L.). This artificial segment has the advantage of a radial homogeneous sap flux density profile and, given the high porosity, allowed a wide range of sap flux densities to be applied. The segment was installed in a verification system as proposed by Steppe *et al.* (2010) (Fig. S2). Flow rates of water were held constant by maintaining a constant head of water pressure on the segment using Mariotte's bottle principle (McCarthy, 1934). A closed water-filled 5-l Erlenmeyer flask was equipped with two glass tubes located at the same depth in the flask: one tube functioned as an air inlet, whereas the other, connected to a third glass tube via flexible tubing, functioned as a siphon. By adjusting the height of the flask (and thus the bottom of the air inlet), the water-filled siphon delivered the flow of water required to maintain a constant head (h, distance between the bottom of the air inlet and the surface of the segment) on the segment, regardless of the changing water level within the flask. Water passing through the segments was continuously measured using an electronic balance (PS 4500/C1, Henk Maas Weegschalen BV, Veen, the Netherlands). At the end of the measurements, the volume of the sawdust column was determined and the sawdust was dried and weighed to determine the dry wood density. As high flows for this artificial column were expected, a needle configuration of (10,0), (− 5,0) and (0,5) mm was applied for the axial downstream, axial upstream and tangential needle, respectively, enabling comparison with CHPM.

Measurements of the sap flux density in sapwood

In addition to the artificial segment, the method was tested in sapwood of European beech (*Fagus sylvatica* L.). To this end, two trees, *c.* 15 yr old, with a diameter at breast height of *c.* 12 cm, were cut at the experimental forest 'Aelmoeseneie' of Ghent University (Gontrode, Belgium). The cut ends were sealed with parafilm (Parafilm M, SPI supplies/Structure Probe Inc., West Chester, PA, USA) and enclosed in plastic bags to minimize evaporation. The stems were then transported to the Laboratory of Plant Ecology, Ghent University, and cut into segments of *c.* 20 cm in length.

Before installing the cut stem segments in the experimental set-up, the cut surfaces were wetted and trimmed using a razor blade to re-open possibly closed vessels (this was visually confirmed using a stereomicroscope). A 2-cm strip of bark at the top end of the segment was removed to ensure that water only passed through the stem xylem. On these segments, a 30-cm-high plastic cylinder was fixed directly to the xylem using silicone and double-sticking adhesive tape. After a drying phase of *c.* 18 h for the silicone to harden, the Sapflow+ sensor was installed. Accurate vertical spacing and parallel drilling was achieved using a drill-bit holder. It should be noted that, before installing the sensors, the bark was removed to ensure that the heater was completely located in the sapwood.

At the end of the experiment, a small disc of the segment was cut from which the volume, moist weight and dry weight after drying for 24 h in a 50°C oven were determined. From these values, the water content and dry wood density were calculated. Moreover, the segment was cut through at the needle position to accurately determine the exact spacing between the measurement needles. As lower flows were expected in comparison with the artificial column, it was preferred to compare the Sapflow+ results with HRM. As it was noted that, for distances of 10 mm, the axial downstream signal was rather low, which reduces the sensitivity of HRM, a smaller distance of 7.5 mm was chosen, resulting in a needle configuration of *c.* (7.5,0), (− 7.5,0) and (0,7.5) mm for the axial downstream, axial upstream and tangential needles, respectively. The following equation for HRM was applied:

$$V_h = \frac{4 D_{ax}\, t \ln(\Delta T_{down}/\Delta T_{up}) - x_{down}^2 + x_{up}^2}{2t(x_{up} - x_{down})} \qquad \text{Eqn 12}$$

(D_{ax}, thermal diffusivity ($m^2\ s^{-1}$); ΔT_{down} and ΔT_{up}, downstream and upstream temperature differences, respectively, at time t after application of the pulse; x_{down} and x_{up}, exact axial downstream and upstream distances, respectively, of the measurement needles to the heater). The thermal diffusivity was

determined according to Cohen *et al.* (1981), as it has been shown that the original method for the determination of *D*, presented in Burgess *et al.* (2001), is incorrect (Vandegehuchte & Steppe, 2012a).

Statistical tests were performed in TIBCO Spotfire S + 8.2.

Results

Identifiability analysis

Figure 2(a–c) shows the relative sensitivity functions for the ΔT signals at positions (10 mm, 0 mm), (− 5 mm, 0 mm) and (0 mm, 5 mm), respectively, from the heater needle. The sensitivity functions of the parameters are clearly different for the different measurement positions. For instance, a positive V_h will have a negative relative sensitivity for positions upstream and tangentially from the heater, whereas the relative sensitivity will be (partly) positive for downstream positions. K_{ax}, however, will have a positive relative sensitivity for axial positions, but negative for the tangential position, and vice versa for K_{tg}. Figure 2(d) gives an indication of the overall sensitivity of the parameters for different heat velocities. It should be noted that, for zero flow, the sensitivity measure for V_h is much lower than for the other parameters (not visible in Fig. 2d). A 1% change in V_h will hardly influence the ΔT signals if V_h is approximately 0. Nevertheless, the model remains practically applicable as an error of 1% in the V_h determination for such a low value is negligible and, for higher absolute V_h values, the sensitivity increases rapidly. Moreover, as the collinearity index remains below 8.5 across the complete natural range of water contents and sap flux densities (from − 15 to 110 $cm^3\ cm^2\ h^{-1}$; Vertessy *et al.*, 1997; Burgess & Bleby, 2006; Cohen *et al.*, 2008), the model can be considered to be identifiable if the heat input and measurement positions are known.

Sensor verification and calibration

Figure 3(a) shows the temperatures obtained with FEM for a distance of 7.5 mm from the heater in immobilized water. As this medium is isotropic, exactly the same results are obtained

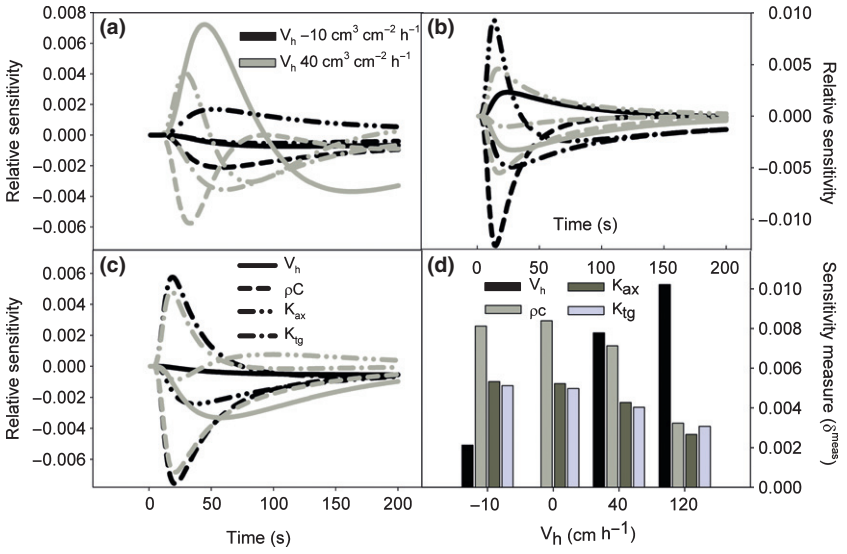

Fig. 2 Relative sensitivity functions for the heat velocity (V_h; black, − 10 $cm^3\ cm^{-2}\ h^{-1}$; grey, 40 $cm^3\ cm^2\ h^{-1}$), volumetric heat capacity (ρc; 2.4×10^6 J m^{-3} K^{-1}), axial thermal conductivity (K_{ax}; 0.62 W m^{-1} K^{-1}) and tangential thermal conductivity (K_{tg}; 0.42 W m^{-1} K^{-1}) for positions 10 mm, 0 mm (a), − 5 mm, 0 mm (b) and 0 mm, 5 mm (c) with reference to the heater. The sensitivity measures for all parameters are given in (d) for different heat velocities.

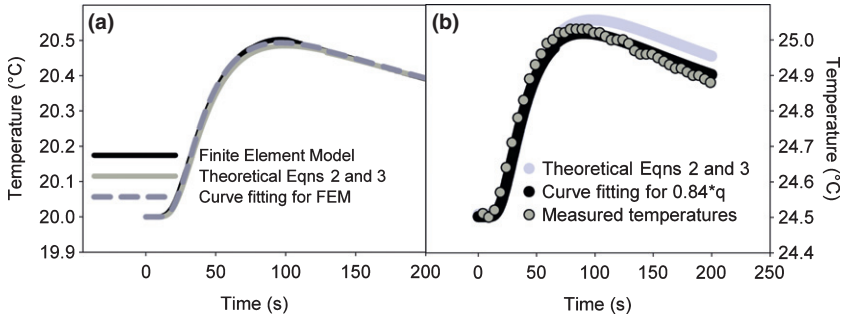

Fig. 3 (a) Temperature data at 7.5 mm from the heater for the finite element model (FEM) of immobilized water compared with the theoretical Eqns 2 and 3 for the thermal properties of water ($\rho c = 4.186 \times 10^6$ J m^{-3} K^{-1}, $K_{ax} = K_{tg} = 0.61$ W m^{-1} K^{-1}, $V_h = 0$ $m^3\ m^{-2}\ s^{-1}$), and the application of Sapflow+ to the FEM data. (b) Measured temperatures with the Sapflow+ sensor in immobilized water compared with the fitted temperatures for *q* calculated according to Campbell *et al.* (1991) and, after calibration for *q*, leading to an optimal value of 0.84**q*. For both FEM and the actual measurements, a heat pulse of 6 s and 160 W m^{-1} was applied.

whether the measurement needle is located axially or tangentially from the heater. Compared with the theoretical Eqns 2 and 3, there is only a small difference in temperatures obtained by FEM (Fig. 3a). The small differences are probably a result of the fact that, in the latter, actual needles are implemented with finite boundaries of a specific material, i.e. stainless steel. When applying Sapflow+ to the FEM data, the following values are obtained (relative difference from the actual values is indicated in parentheses): ρc, 4.108×10^6 J m^{-3} K^{-1} (− 1.8%); K_{ax}, K_{tg}, 0.6176 W m^{-1} K^{-1} (+1.2%); V_h, 0 m^3 m^{-2} s^{-1}.

In Fig. 3(b), actual measurements with the Sapflow+ sensor in immobilized water are given. As, for the three measurement needles at (0,7.5), (7.5,0) and (− 7.5,0) mm from the heater, similar temperatures were obtained, the data are only plotted for one needle. When comparing these measurements with Eqns 2 and 3, the theory seems to overestimate the temperature. If, however, the heat input q, as calculated according to Campbell *et al.* (1991), is reduced, a good fit is obtained (objective value of 13.17 compared with 12 for an ideal fit).

Figure 4 stresses the importance of temperature correction. During the measurement, the ambient conditions generally change during the day, influencing the measured temperature peaks (Fig. 4a). Without temperature correction, application of the presented method would lead to erroneous results. Figure 4(b) shows the curve fitting without calibration for the known thermal parameters of stabilized water when no temperature correction is applied. When calibrating the parameters of Eqns 2 and 3 to obtain a good fit, erroneous results are obtained ($\rho c = 4.344 \times 10^6$ J m^{-3} K^{-1} (+4%); $K_{ax} = K_{tg} =$ 0.824 W m^{-1} K^{-1} (+ 34%)) and the fit has an objective value of 694 compared with 2.54 for an ideal fit. If, however, a temperature correction is applied, the method is again able to correctly determine the desired variables from the curve-fitting procedure. The data shown have been corrected for temperature effects.

Comparison of heat-pulse methods by FEM

In Fig. 5(a), the calculated heat velocities according to the Sapflow+, Tmax, CHPM and HRM are given for FEM of sapwood without wound effects. Similar results were obtained for other water contents and dry wood densities. Figure 6 shows that, for HRM measurements at high heat velocities, the upstream ΔT signal is nearly zero, whereas the downstream ΔT signal is lower than for lower heat velocities between 60 and 100 s, the time period for calculating the average $\Delta T_{down}/\Delta T_{up}$ signal.

In addition to accurately determining the heat velocity, Table 2 indicates that the Sapflow+ method is also capable of accurately estimating the water content of the sapwood, a crucial parameter for the conversion of the heat velocity to the sap flux density. Moreover, the thermal conductivities of the sapwood are estimated, although less accurately, as the method is less sensitive to these parameters.

In practice, however, sap flux density measurements are influenced by wound effects. Figure 5(b) shows the modelling results when wound effects are introduced, which more closely correspond to reality in comparison with Fig. 5(a). Clearly, all methods are affected. When fitting a linear regression, the Sapflow+ method leads to the best fit and highest slope, although the R^2 value does not differ greatly compared with the other methods (Table 3). When regressing the difference between the Sapflow+ results and the results of the other methods, the slopes are all significantly different from zero, indicating a significant difference between Sapflow+ and the other methods. For both the CHPM and Tmax method, the intercept is also significantly different from zero. Moreover, the R^2 value for the regressed difference between Sapflow+ and HRM is only 0.566 because of the inaccurate HRM results at high heat velocities (Table 3). The main difference, however, lies in the applicability of the methods across the sap flow range. The Sapflow+ method is the only method leading to good results for negative, low as well as high heat velocities. Hence, by applying a simple linear wound correction (as can be seen in Fig. 5b), accurate heat velocities across the entire range of sap flux densities can be determined by this method. The wound effect, however, also influences the calculated thermal parameters, and hence water content (Fig. 7). For low heat velocities ranging between − 15 and 45 cm h^{-1}, the thermal parameters and water content are determined accurately (relative error < 5%). For larger absolute heat velocities, however, the relative errors increase and become more dependent on the

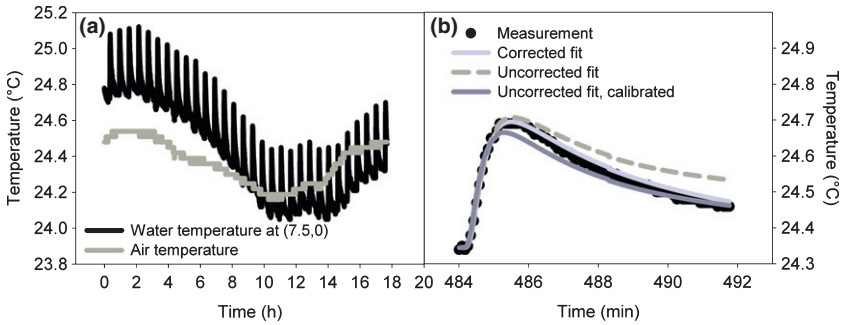

Fig. 4 (a) Measured air temperature and temperature in immobilized water at location (7.5, 0) mm from the heater for heat pulses of 6 s and 105 W m^{-1}, applied every 45 min. (b) Measured water temperature for one heat pulse compared with the curve fitting for $\rho c = 4.186 \times 10^6$ J m^{-3} K^{-1} and $K_{ax} = K_{tg} = 0.61$ W m^{-1} K^{-1} with and without temperature correction. When calibrating the fitted curve without temperature correction, values of 4.344×10^6 J m^{-3} s^{-1} (+4%) for ρc, 0.824 W m^{-1} K^{-1} (+34%) for K_{ax} and K_{tg}, and 0 m^3 m^{-2} s^{-1} for V_h are obtained.

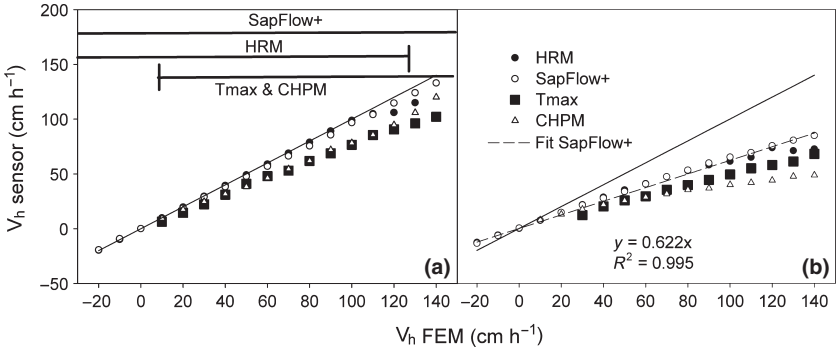

Fig. 5 Heat velocity calculated according to the heat ratio method (HRM), Tmax method (Tmax), compensation heat-pulse method (CHPM) and Sapflow+ based on the temperature data obtained by the finite element model for sapwood with a dry wood density of 550 kg m^{-3} and a water content of 0.75 without (a) and with (b) the wound effect. The heat velocity range for which each method is applicable is indicated. The solid line indicates the 1 : 1 line.

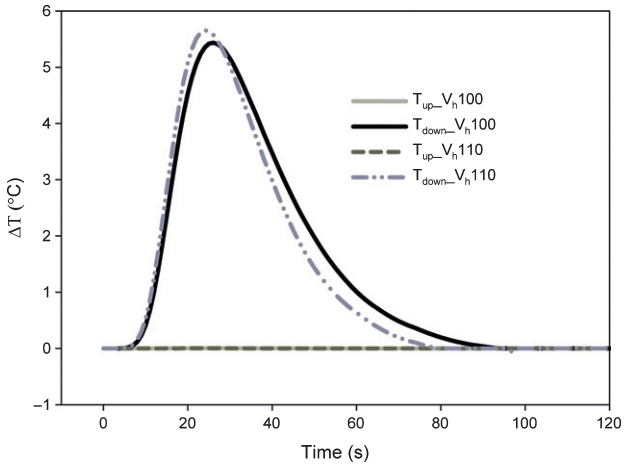

Fig. 6 The ΔT_{up} and ΔT_{down} heat ratio method (HRM) signals for heat velocities of 100 and 110 cm h^{-1}. Although, for the ΔT_{up} signal, the difference for both flows is hardly noticeable, the ΔT_{down} signal between 60 and 100 s is clearly higher for V_h = 100 cm h^{-1}.

Table 2 Water content (MC), axial and tangential conductivity (K_{ax}, K_{tg}) implemented in the finite element sapwood model (FEM) and the corresponding average values for heat velocities from − 20 to 140 cm^3 cm^{-2} h^{-1} calculated with the Sapflow+ method (SF+)

MC FEM	MC SF+	K_{ax} FEM	K_{ax} SF+	K_{tg} FEM	K_{tg} SF+
0.748	0.748 (± 0.013)	0.6275	0.607 (± 0.014)	0.42	0.46 (± 0.0230)
0.855	0.861 (± 0.007)	0.6634	0.637 (± 0.030)	0.44	0.467 (± 0.022)
0.955	0.921 (± 0.016)	0.6964	0.663 (± 0.028)	0.46	0.467 (± 0.018)
1.045	1.04 (± 0.007)	0.7263	0.687 (± 0.048)	0.48	0.511 (± 0.027)

Standard deviation is shown in parentheses.

water content. Based on the modelling results, however, a nonlinear correction can be applied based on the pooled data for all water contents which will reduce the error to a maximum of 7%.

Measurements on artificial sapwood

Figure 8(a) shows the heat velocity calculated according to the Sapflow+ method and CHPM in comparison with the gravimetric heat velocity for the artificial column. As no direct measurement of MC was possible on the artificial column, the value determined by the Sapflow+ method for zero flow was applied for all measurements, given the negligible error for MC determination during zero flow in the modelling results. This value was also applied to calculate the gravimetric heat velocity from the measured gravimetric sap flux density. In Fig. 8(b), the relative error in MC determined by Sapflow+, with the zero flow determined by Sapflow+ taken as reference, is given. Again, the error increases with increasing heat velocity because of the interruption of flow around the needles (wound effect).

Measurements on sapwood

For real sapwood segments of European beech (*Fagus sylvatica*), a maximal heat velocity (derived from the sap flux density, dry wood density and water content of the sapwood according to Eqn 1) of 45 cm h^{-1} was obtained (Fig. 9a). Regressing the Sapflow+ and HRM results to the heat velocity led to a slope of 0.61 and R^2 of 0.982 for HRM, and 0.61 and 0.978, respectively, for Sapflow+. Hence, for heat velocities up to 45 cm h^{-1}, HRM and Sapflow+ perform equally. This was confirmed by linear regression of the

Table 3 Linear regression results of the different heat-pulse methods resulting from the finite element sapwood model with wound effects

	SF+	HRM	Tmax	CHPM	SF+-HRM	SF+-Tmax	SF+-CHPM
Slope	0.62*	0.56*	0.48*	0.31*	0.057*	0.100*	0.294*
Intercept	1.56	3.18	0.40	8.47*	−1.62	4.857*	−4.847*
R^2	0.997	0.979	0.994	0.981	0.567	0.871	0.995

Results were regressed against the implemented heat velocity V_h. Significant results are indicated by *. SF+, Sapflow+ method; HRM, heat ratio method; Tmax, Tmax method; CHPM, compensation heat-pulse method.

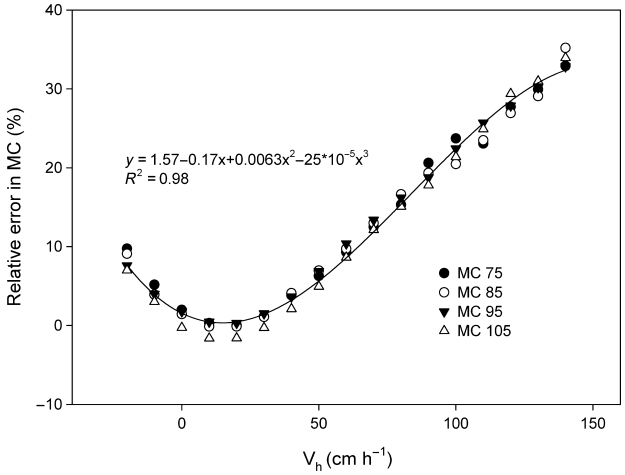

Fig. 7 Relative error (%) of the water content (MC), calculated as the difference in water content determined by the Sapflow+ method and the model input water content divided by the model input water content, for different water contents and heat velocities.

difference in the Sapflow+ and HRM results to the gravimetric heat velocity, which did not lead to a significant slope (P = 0.824) or intercept (P = 0.697) (Fig. 10). Nevertheless, differences between stem segments can be noted (Table 4). It should be noted that, for both methods, measurements were only performed at a single sapwood depth. Although the relative error in the calculated water content was, on average, 0.8 ± 1.4% for zero flow conditions, it increased to 10% for higher heat velocities (Fig. 9b).

Discussion

Applicability of the Sapflow+ method

From the identifiability analysis, the model is theoretically able to correctly determine V_h, ρc, K_{ax} and K_{tg} across the entire natural range of sapwood water contents and sap flux densities. This was also confirmed by the results of FEM (Fig. 3a). For the measurements in stabilized water, the fit was not as accurate as for FEM, unless the heat input was reduced in the Sapflow+ model (Fig. 3b). As the heater needles are manufactured manually, the heater wire is not entirely inserted in the wood to facilitate coupling to the voltage source. Moreover, it is likely that some of the generated heat is taken up by the heater material itself and hence not given off to the surrounding wood. Therefore, a calibration in immobilized water, for which the thermal characteristics are known, is necessary to correct the parameter q for every sensor. As q is only dependent on the heater needle itself and not on the thermal characteristics of the sapwood, this sensor-specific correction will be applicable for all further measurements.

In addition to a correct heat input, precise positioning of the sensor needles needs to be known to obtain good results, which was also mentioned by Swanson (1983), Jones *et al.* (1988) and, later, by Kluitenberg *et al.* (1995) for other heat-pulse-based methods. A 5% error in needle spacing can lead to an error of up to 16% in the calculated heat velocities and MC, with the error depending on the heat velocity and being relatively larger for

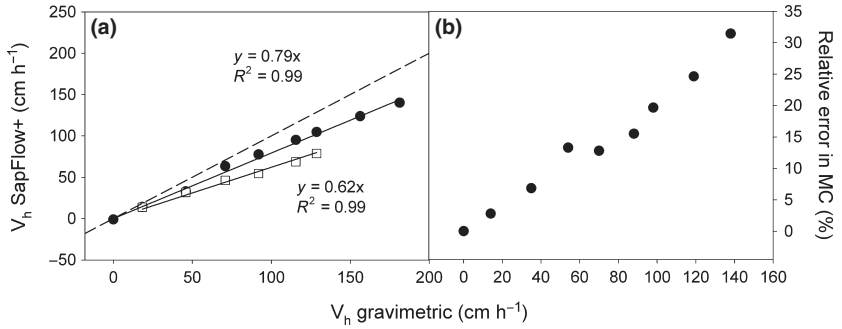

Fig. 8 (a) Heat velocity (V_h) in the artificial column calculated by Sapflow+ (circles) and the compensation heat-pulse method (CHPM; squares) in comparison with the gravimetric heat velocity (determined from the gravimetric sap flux density based on the water content calculated by Sapflow+ for zero flow). The broken line indicates the 1 : 1 line. (b) Relative error in water content (MC) determination by Sapflow+ with the zero flow measurement as reference value.

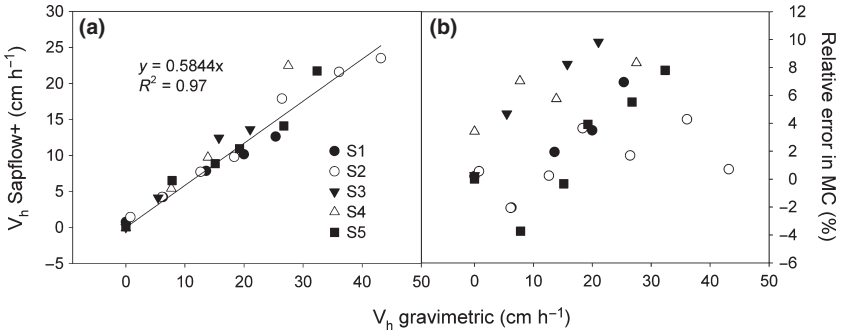

Fig. 9 (a) Heat velocity (V_h) in the stem segments calculated by Sapflow+ in comparison with the gravimetric heat velocity. (b) Relative error in water content (MC) determination by the Sapflow+ method with the gravimetrically determined water content as reference value.

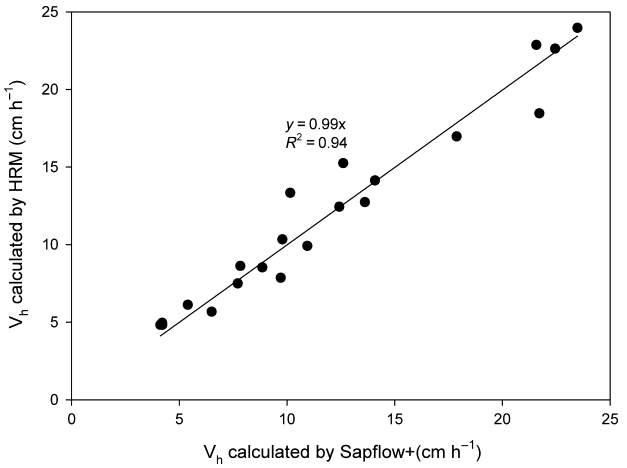

Fig. 10 Heat velocity (V_h) calculated by the heat ratio method (HRM) vs heat velocity calculated by the Sapflow+ method for all sapwood segments.

Table 4 Linear regression results for the Sapflow+ method applied for the different stem segments as shown in Fig. 9

	S1	S2	S3	S4	S5
Slope	0.46*	0.55*	0.68*	0.82*	0.60*
Intercept	1.1*	0.97	0.40	−0.73	0.29
R^2	0.995	0.980	0.976	0.994	0.953

Significant results are indicated by *.

lower flows (Supporting Information Table S1). Similar error percentages were obtained for other MC values. It is thus recommended to use a template to install the needles in the sapwood. In addition, a fixed sensor design can aid users to avoid spacing errors, especially as needle spacings during calibration and measurements need to be equal.

Comparison of Sapflow+ with other heat-pulse methods

Similar to previous studies (Swanson, 1983; Green *et al.*, 2003), the FEM results (Fig. 5) show that Tmax and CHPM are not capable of determining negative or low heat velocities (<5 cm h^{-1}), which was also confirmed for CHPM in the artificial stem segment data (Fig. 8a). Moreover, both Tmax and CHPM underestimate V_h, even without modelled wound effects. For CHPM, this was expected, as the applied equation is not strictly valid for nonideal pulses, which can be seen as a general shortcoming of the method because, in practice, pulses will never be ideal. Apparently, the Tmax method is more sensitive to the probe material than are Sapflow+ or HRM, for which the results agree closely with the 1 : 1 line without wounding. HRM, furthermore, can resolve reverse and low heat velocities (Figs 5, 9a) and agrees well with Sapflow+ for the stem segment measurements (Fig. 10), but shows deviations for high heat velocities (> 110 cm h^{-1}) in the modelling results (Fig. 5). For these high heat velocities, the HRM heat velocity levels off or even decreases as ΔT_{up} remains approximately the same, whereas ΔT_{down} decreases slightly between 60 and 100 s (Fig. 6). Shifting the time period for which the average HRM signal was calculated led to slightly better, but still inadequate, results for the higher heat velocities; this was also indicated by Green *et al.* (2009), who stated that shortening the averaging window or altering the probe spacing does not largely improve the measurement range of HRM. Moreover, for very high heat velocities, the ΔT_{up} signal becomes so small that the $\Delta T_{down}/\Delta T_{up}$ signal reaches extremely high values, leading to absurdly high heat velocity results. In practice, these flaws will worsen the applicability of HRM, as ΔT signals below 0.02°C are smaller than the detection limit of most thermometric systems. Generally, a maximum heat velocity of *c.* 55 cm h^{-1} is presumed to be measurable with HRM (Swanson, 1983; Burgess *et al.*, 2001). A similar experiment for segments which allow higher sap flux densities would be beneficial to assess the difference between HRM and Sapflow+ for higher flows. For these flows, the Sapflow+ method could make a difference, as it does not suffer from these sensitivity problems because three measurement needles are applied. In this way, the heat velocity can be accurately determined across the entire range of sap flux densities when applying wound correction (Figs 5, 9a). Given the symmetric positioning of the axial temperature sensors, it can be assumed that good results will also be obtained for reverse flow in stem segments, as the only difference will be that the upstream sensor needle will become the downstream needle, and vice versa. The smaller underestimation for the artificial stem segment in comparison with the stem segments (Figs 8a, 9a) is probably a result of the larger pores, allowing water to continue its flow path more easily around the sensor needles, which results in a smaller wound effect.

In addition to its applicability across the entire range of sap flux density, the Sapflow+ method has the advantage that, unlike Tmax or HRM, thermal diffusivity does not need to be determined separately as it is included in the model calibrations. Hence, thermal diffusivity will be a model output instead of an input, which is known to be prone to errors (Green *et al.*, 2003; Vandegehuchte & Steppe, 2012a). Another advantage is that the water content is simultaneously and accurately estimated with heat velocity with Sapflow+, at least for low flows ranging between − 15 and 45 cm h^{-1}. Hence, unlike other methods, which determine the sap flux density from the heat velocity by measuring the sapwood water content only once (taking a destructive wood core), Sapflow+ enables regular updates of water content values, which will lead to more accurate sap flux densities. At higher heat velocities, less heat is transported tangentially and radially, resulting in a narrower and axially longer heat field in comparison with lower heat velocities. As the area in which flow is interrupted by wounding lies within this narrow zone, the influence of this area will become more important, in comparison with a broader heat field for lower heat velocities. When applying the nonlinear correction (Fig. 7), even estimations of water content changes at higher heat velocities can be made, although these will probably be less accurate, as wound effects may vary depending on wood characteristics.

Challenges for the Sapflow+ method

The regression results for the separate stem segments show clear differences (Table 4). This is probably a result of radial and azimuthal variation in flow within the segments. As not only variation between trees, but also within the sapwood of a single tree, can occur as a result of stress factors, measurements at different depths seem indispensable. The application of multiple thermocouples at different depths could easily solve this, as has been shown for HRM, for which the commercial sensors enable measurements at two radial depths. Hence, given a more complicated fabrication of the sensors, Sapflow+ should be able to allow measurements at multiple depths.

Overall, the results indicate that Sapflow+ performs well in determining the heat velocity across the entire naturally occurring sap flow range (*c.* − 15 to 110 $cm^3\ cm^2\ h^{-1}$) and water content at low flows (V_h < 45 $cm\ h^{-1}$), necessary for the conversion of the heat velocity to the sap flux density. Nevertheless, wound corrections are required to overcome the underestimations of heat velocity and water content determinations at higher flows. Thus far, existing wound corrections for the current available sap flow measurement methods are based on models similar to FEM used in this study (Swanson & Whitfield, 1981; Burgess *et al.*, 2001). However, as wound effects seem to play a significant role in the performance of heat-pulse-based sensors and the correction factors that need to be applied, further research on this topic seems to be essential to obtain more accurate results. It seems likely that wound effects not only depend on needle diameters, but also on wood characteristics, which vary between and within tree species, and might be influenced by the heating process itself. Therefore, a combination of modelling, gravimetric validation experiments and more advanced methods, such as MRI, should be applied to increase our knowledge with regard to these wound phenomena and to enable accurate wound corrections for different wood types.

Acknowledgements

The authors wish to thank the Fund for Scientific Research-Flanders (FWO) for the PhD grant awarded to M.W.V. We also wish to thank Geert Favyts and Philip Deman for their indispensable technical aid during the construction of the sensors. We would also like to thank Todd Dawson and two other anonymous reviewers for their helpful comments which improved the manuscript.

References

Becker P. 1998. Limitations of a compensation heat pulse velocity system at low sap flow: implications for measurements at night and in shaded trees. *Tree Physiology* **18**: 177–184.

Bieker D, Rust S. 2012. Electric resistivity tomography shows radial variation of electrolytes in *Quercus robur*. *Canadian Journal of Forest Research* **40**: 1189–1193.

Burgess SSO, Adams M, Turner NC, Beverly CR, Ong CK, Khan AAH, Bleby TM. 2001. An improved heat pulse method to measure low and reverse rates of sap flow in woody plants. *Tree Physiology* **21**: 589–598.

Burgess SSO, Bleby TM. 2006. Redistribution of soil water by lateral roots mediated by stem tissues. *Journal of Experimental Botany* **57**: 3283–3291.

Burgess SSO, Dawson TE. 2008. Using branch and basal trunk sap flow measurements to estimate whole-plant water capacitance: a caution. *Plant and Soil* **305**: 5–13.

Campbell GS, Calissendorff C, Williams JH. 1991. Probe for measuring soil specific-heat using a heat-pulse method. *Soil Science Society of America Journal* **55**: 291–293.

Clearwater MJ, Luo ZW, Mazzeo M, Dichio B. 2009. An external heat pulse method for measurement of sap flow through fruit pedicels, leaf petioles and other small-diameter stems. *Plant, Cell & Environment* **32**: 1652–1663.

Cohen Y, Cohen S, Cantuarias-Aviles T, Schiller G. 2008. Variations in the radial gradient of sap velocity in trunks of forest and fruit trees. *Plant and Soil* **305**: 49–59.

Cohen Y, Fuchs M, Green GC. 1981. Improvement of the heat pulse method for determining sap flow in trees. *Plant, Cell & Environment* **4**: 391–397.

De Pauw DJW, Steppe K, De Baets B. 2008. Identifiability analysis and improvement of a tree water flow and storage model. *Mathematical Biosciences* **211**: 314–332.

Edwards WRN, Warwick NWM. 1984. Transpiration from a kiwifruit vine as estimated by the heat pulse technique and the Penman–Monteith equation. *New Zealand Journal of Agricultural Research* **27**: 537–543.

Granier A. 1985. Une nouvelle méthode pour la mesure du flux de sève brute dans le tronc des arbres. *Annales Scientifique Forestières* **42**: 193–200.

Green S, Clothier B, Jardine B. 2003. Theory and practical application of heat pulse to measure sap flow. *Agronomy Journal* **95**: 1371–1379.

Green S, Clothier B, Perie E. 2009. A re-analysis of heat pulse theory across a wide range of sap flows. In: Fernandez JE, Diaz-Espejo A, eds. *7th International Workshop on Sap Flow*. Seville, Spain: Acta Horticultura, 95–104.

Huber B. 1932. Beobachtung und messung pflanzlicher saftstrome. *Berichte der Deutschen Botanischen Gesellschaft* **50**: 89–109.

Jones HG, Hamer PJC, Higgs KH. 1988. Evaluation of various heat-pulse methods for estimation of sap flow in orchard trees: comparison with micrometeorological estimates of evaporation. *Trees – Structure and Function* **2**: 250–260.

Jones M, Aptaker PS, Cox J, Gardiner BA, McDonald PJ. 2012. A transportable magnetic resonance imaging system for *in-situ* measurements of living trees: the tree hugger. *Journal of Magnetic Resonance* **218**: 133–140.

Kluitenberg GJ, Bristow KL, Das BS. 1995. Error analysis of heat pulse method for measuring soil heat-capacity, diffusivity and conductivity. *Soil Science Society of America Journal* **59**: 719–726.

Kluitenberg GJ, Ham JM. 2004. Improved theory for calculating sap flow with the heat pulse method. *Agricultural and Forest Meteorology* **126**: 169–173.

Marshall DC. 1958. Measurement of sap flow in conifers by heat transport. *Plant Physiology* **33**: 385–396.

Martin LH, Lang KC. 1933. The thermal conductivity of water. *Proceedings of the Physical Society* **45**: 523–529.

McCarthy EL. 1934. Mariotte's bottle. *Science* **80**: 100.

Nadezhdina N, Cermak J, Nadezhdin V. 1998. Heat field deformation method for sap flow measurements. In: Cermak J, Nadezhdina N, eds. *Proceedings of the 4th International Workshop on Measuring Sap Flow in Intact Plants*. Brno, Czech Republic: Publishing House of Mendel University, 72–92.

Nadezhdina N, Vandegehuchte M, Steppe K. 2012. Sap flux density measurements based on the heat field deformation method. *Trees – Structure and Function*. doi: 10.1007/s00468-012-0718-3.

Nadler A, Raveh E, Yermiyahu U, Lado M, Nasser A, Barak M, Green S. 2008. Detecting water stress in trees using stem electrical conductivity measurements. *Soil Science Society of America Journal* **72**: 1014–1024.

Nadler A, Tyree MT. 2008. Substituting stem's water content by electrical conductivity for monitoring water status changes. *Soil Science Society of America Journal* **72**: 1006–1013.

Nelder JA, Mead R. 1965. A simplex method for function minimization. *Computer Journal* **7**: 308–313.

Ren T, Ochsner TE, Horton R, Ju Z. 2003. Heat-pulse method for soil water content measurement. *Soil Science Society of America Journal* **67**: 1631–1634.

Skaar C, ed. 1988. *Wood–water relations*. New York, NY, USA; Berlin, Heidelberg, Germany: Springer.

Steppe K, De Pauw DJW, Doody TM, Teskey RO. 2010. A comparison of sap flux density using thermal dissipation, heat pulse velocity and heat field deformation methods. *Agricultural and Forest Meteorology* **150**: 1046–1056.

Steppe K, De Pauw DJW, Lemeur R, Vanrolleghem PA. 2006. A mathematical model linking tree sap flow dynamics to daily stem diameter fluctuations and radial stem growth. *Tree Physiology* **26**: 257–273.

Swanson RH. 1983. *Numerical and experimental analyses of implanted-probe heat pulse velocity theory*. PhD thesis, University of Alberta, Edmonton, AB, Canada.

Swanson RH, Whitfield DWA. 1981. A numerical analysis of heat pulse velocity theory and practice. *Journal of Experimental Botany* **32**: 221–239.

Testi L, Villalobos FJ. 2009. New approach for measuring low sap velocities in trees. *Agricultural and Forest Meteorology* **149**: 730–734.

Van As H, Scheenen T, Vergeldt FJ. 2009. MRI of intact plants. *Photosynthesis Research* **102**: 213–222.

Vandegehuchte MW, Steppe K. 2012a. Improving sap flux density measurements by correctly determining thermal diffusivity, differentiating between bound and unbound water. *Tree Physiology*. doi: 10.1093/treephys/tps034.

Vandegehuchte MW, Steppe K. 2012b. Unveiling the heat field deformation method: erroneous use of thermal diffusivity and need for a correction equation in sap flux measurements. *Agricultural and Forest Meteorology* **162–163**: 91–97.

Vandegehuchte MW, Steppe K. 2012c. Use of the correct heat conduction–convection equation as basis for heat-pulse sap flow methods in anisotropic wood. *Journal of Experimental Botany* **63**: 2833–2839.

Vertessy RA, Hatton TJ, Reece P, O'Sullivan SK, Benyon RG. 1997. Estimating stand water use of large mountain ash trees and validation of the sap flow measurement technique. *Tree Physiology* **17**: 747–756.

Wullschleger SD, Hanson PJ, Dawson TE. 1996. Measuring stem water content in four deciduous hardwoods with a time-domain reflectometer. *Tree Physiology* **16**: 809–815.

Supporting Information

Additional supporting information may be found in the online version of this article.

Fig. S1 Geometric configuration of the finite element model with the heater and the axial and tangential measurement needles of the Sapflow+ sensor.

Fig. S2 Schematic diagram of the Mariotte-based verification system (from Steppe *et al.*, 2010) used for testing the accuracy of the Sapflow+ method.

Table S1 Error analysis for varying distances

Notes S1 Identifiability analysis

Please note: Wiley-Blackwell are not responsible for the content or functionality of any supporting information supplied by the authors. Any queries (other than missing material) should be directed to the *New Phytologist* Central Office.